Adaptive combined DE/FE algorithm for analyzing impact fracture problem

Wei Xu* and Jiro Sakamoto

School of Mechanical Engineering, College of Science and Engineering, Kanazawa University, Kanazawa, 920-1192, Japan
*Corresponding and presenting author: xwteamobj007@gmail.com

Abstract

This paper presents a description of a 3D adaptive combined DE/FE algorithm which can automatically convert the distorted finite elements into the spherical discrete elements during simulating the impact fracture of laminated glass. In this method a system is completely discretized into the finite elements at the initial moment without any discrete element existing until part of the finite elements becoming severely deformed. Subsequently each finite element, whose maximum tensile stress exceeds a user-specified conversion criterion, is converted into eight spherical discrete elements. At the same time the system is fragmented into two subdomains, the finite element (FE) and the discrete element (DE) subdomains. The impact fracture of a glass beam is simulated by the adaptive algorithm and the discrete element method, respectively. A satisfactory agreement of the simulation results is observed which validates the feasibility of such an adaptive algorithm; however, the computational efficiency of the adaptive algorithm is much higher than that of latter.

Keywords: Combined algorithm; Brittle fracture; Cohesive model; Discrete element method; Laminated glass

Introduction

Laminated glass generally consists of two or more layers of glass sheets combined by the elastomeric interlayers of Polyvinyl Butyral (PVB) under heat treatment and has been wildly used in automobile windshields, modern buildings, etc. thanks to its security and durability performance. The mechanical properties of laminated glass are more complicated than those of single glass due to the brittleness of glass, the hyper-elasticity of PVB interlayer and the coupled influence of both formers.

The fracture behavior and the flexural strength of laminated glass were not only influenced by the flexural stiffness of each layer but also by their interfacial bonding strength. A parametric study was carried out by Hidallana-Gamage et al. to investigate the influence of structural sealant joints on the mechanical properties of laminated glass panels under blast loading, the information in which might be employed to complement the guidance in the existing design standards [Hidallana-Gamage et al (2014)]. Foraboschi implemented the sacrificial ply design concept to design laminated glass in which the outer glass as a sacrificial ply was permitted to damage under small impact while the inner was designed to remain unbroken [Foraboschi (2007; 2013)]. The fracture behaviors of laminated glass windows subjected to impulsive and blast loadings were experimentally studied with the laboratory airbag pendulum impact tests and the full-scale field blast tests, respectively [Zhang et al (2015)]. The responses of laminated glass in the lab and field tests, such as failure process, applied pressure and deflections, were used to validate the accuracy of the design standards predictions.

Most of numerical studies mentioned above were preceded in the framework of the finite element method (FEM). The contact problem over the crack surfaces and the fragments dispersion might be present, which were of great importance for the fracture of laminated glass. The essence of material fracture was a complicated transi-

tion from continuum to non-continuum. However, it was very difficult to calculate the contact force over the crack surfaces and capture the dispersing fragments in the FEM framework. Fortunately, it was very simple to deal with the transition process by changing the joint types between the DEs in the framework of the discrete element method (DEM). The DEM proposed by Cundall [Cundall (1971)] had been employed to simulate the fracture behavior of brittle materials [Oda and Yasuda (2007); Griffiths and Mustoe (2001); Zang et al (2007); Shan et al (2009)].

To take full advantages of the both numerical methods mentioned above, a 3D adaptive combined DE/FE algorithm has been developed, which can automatically convert the distorted finite elements into the spherical discrete elements during the impact fracture simulations. The detailed description about the 3D adaptive algorithm is presented in Section 2. The corresponding numerical code has been developed in Fortran 90/95 programming language. In Section 3, the fracture simulation is performed on a three-point bending glass beam and the feasibility of the 3D adaptive algorithm is validated by comparing the fracture procedures simulated by the proposed algorithm and the DEM.

Adaptive combined DE/FE algorithm

Introduction of the combined DE/FE method

A continuous elastic solid (solution domain) is considered with the volume Ω and the surface S as shown in Figure 1. It is fragmented into two subdomains, Ω_a and Ω_b with the surfaces $S_{\sigma a}$, S_{ua} and $S_{\sigma b}$, S_{ub} , respectively, which are to be joined together along an interface S_{ab} . Here $S_{\sigma a}$ and $S_{\sigma b}$ are the surfaces prescribed the external forces, S_{ua} and S_{ub} are the surfaces prescribed displacements [Lei and Zang (2010)]. In this work the solution domain is divided into the DE and the FE subregions. The constraint condition between both subregions is enforced on the interface S_{ab} by using the penalty method.

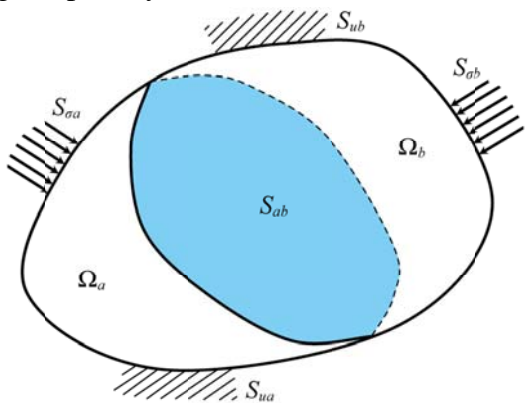


Figure 1. Solution domain divided into two subdomains

The adaptive procedure

Figure 2(a) illustrates a finite element grid with four 8-node cubic FEs (A, B, C and D) on the surface designated as the candidates for conversion into the spherical DEs. In the grid only the nodes 1, 2, 3, ··· 32 are numbered for simplicity. The full integration is employed in the FE model. If the maximum tensile stress of a FE, such as the finite element B, exceeds a user-specified criterion, named the conversion stress, the following five steps are taken to convert it into eight spherical DEs. The conversion keeps the mass, the momentum and the energy conservation laws approximately. The deformation of the FE is approximatively mirrored by the separation or penetration (the relative displacement in the local coordinate) between the DEs; the stress state of the FE by the internal force between the DEs. The internal force is calculated by the spring constants and the relative displacement between the DEs.

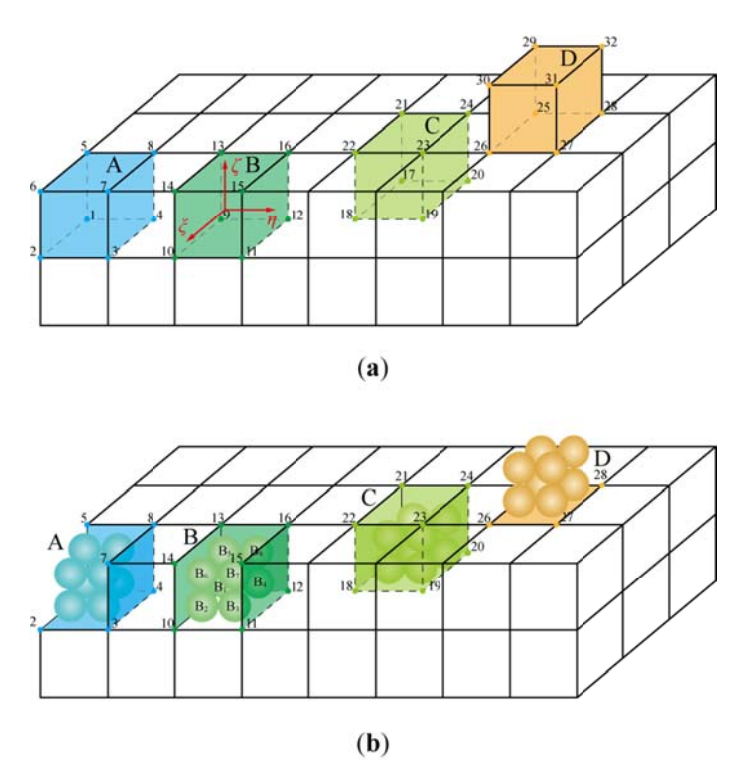


Figure 2. Conversion of the distorted finite elements into the spherical discrete elements. **a** The finite elements before conversion, **b** The finite and discrete elements after conversion

(1) The discrete element B_i ($i = 1, 2, 3, \dots 8$) is generated at the integration point calculated by the interpolation of the nodal positions of the finite element B,

$$\boldsymbol{p}^{l} = \sum_{I} N_{I}(\xi_{i}, \eta_{i}, \zeta_{i}) \boldsymbol{p}^{I}$$
(1)

where p^i is the position of the discrete element B_i ; p^i is the nodal position of the finite element B; $N_I(\xi_i, \eta_i, \zeta_i)$ is the value of the shape function, here (ξ_i, η_i, ζ_i) is the natural coordinate of the center of the discrete element B_i . The radius of each DE is r = l/4, here l is the original edge length of the finite element B.

(2) The mass of the discrete element B_i is set to be $m_f/8$, in which m_f is the mass of the finite element B; the translational displacement and velocity of the discrete element B_i are calculated by the interpolations of the nodal displacements and velocities of the finite element B, respectively:

$$\boldsymbol{u}^{i} = \sum_{I} N_{I}(\xi_{i}, \eta_{i}, \zeta_{i}) \boldsymbol{u}^{I}$$
 (2)

$$\dot{\boldsymbol{u}}^{i} = \sum_{I} N_{I}(\xi_{i}, \eta_{i}, \zeta_{i}) \dot{\boldsymbol{u}}^{I}$$
(3)

in which u^i and \dot{u}^i are the translational displacement and velocity of the discrete element B_i , respectively; u^I and \dot{u}^I are the nodal displacement and velocity of the finite element B, respectively.

(3) The finite element B is removed from the model grid and the nodal mass of the finite element B is also reduced from the FE model. The reduced nodal mass is $m_f/8$. If a node does not belong to any finite element, it should be removed from the nodal

list.

- (4) If the surfaces 13-14-15-16 and 10-11-15-14 of the finite element B contacts with the other parts, they are not effective now and should be removed from the contact surface segments. The contact force calculation is replaced by the contact between the discrete elements B₅-B₆-B₇-B₈ and B₂-B₃-B₇-B₆ and the other parts. The discrete elements B₁, B₂, B₆ and B₅ are combined with the surface 9-10-14-13; B₁, B₄, B₈ and B₅ with the surface 9-12-16-13; B₃, B₄, B₈ and B₇ with the surface 11-12-16-17; B₁, B₂, B₃ and B₄ with the surface 9-10-11-12. The interface force calculation will be introduced in the following subsection.
- (5) The connective joint type between the DEs is guaranteed at the moment when the DEs are generated by setting the conversion stress to be about $(0.90\text{-}0.95)\sigma_t$, slightly smaller than the tensile strength of the brittle material. As shown in Figure 3 the translational displacements of the discrete elements B_i and B_j are \boldsymbol{u}^i and \boldsymbol{u}^j , respectively. The vectors \boldsymbol{d}^i and \boldsymbol{d}^j are employed to record the rotations of the discrete elements B_i and B_j , respectively. The normal and the tangential springs between the DEs are connected by the two points c_i and c_j on the discrete elements B_i and B_j , respectively. Since the rotation of the DE is neglected for the small deformation problems, the two vector $\boldsymbol{d}^i = \boldsymbol{d}^{i'}$ and $\boldsymbol{d}^j = \boldsymbol{d}^{j'}$. Finally the relative displacement $\Delta \boldsymbol{u}^{ij}$ between the discrete elements B_i and B_j in the local coordinate x'y'z' is calculated by the following formula:

$$\Delta \mathbf{u}^{ij} = \mathbf{N} \big(\mathbf{u}^j - \mathbf{u}^i \big) \tag{4}$$

in which N is the transform matrix from the global coordinate xyz to the local coordinate x'y'z'.

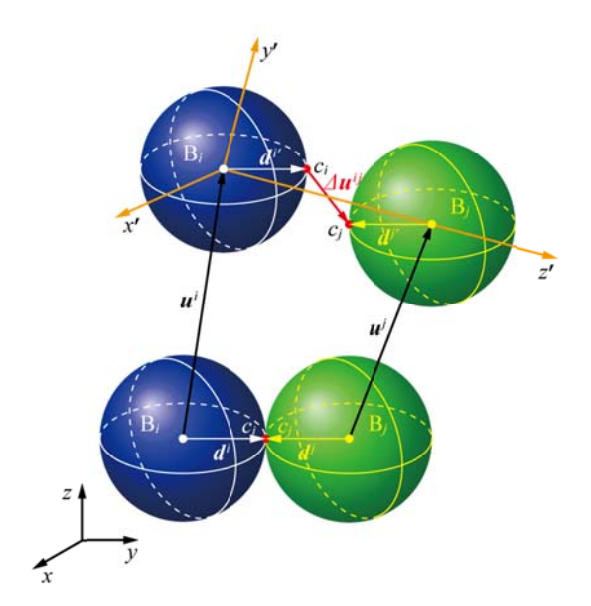


Figure 3. Relative displacement between the discrete elements B_i and B_i

For the conversion of the finite element A, C, and D, most of the steps are similar to those adopted for the finite element B. The final elements configuration after conversion is illustrated in Figure 2(b).

Numerical simulation

In this part, the impact fracture simulations are performed on a three-point bending glass beam by using the 3D adaptive algorithm and the DEM, respectively. The resulting fracture behaviors are compared with each other to validate the feasibility of

the 3D adaptive algorithm whose computational time is compared with that of the DEM to verify the former's higher computational efficiency.

The geometry of the three-point bending glass beam is illustrated in Figure 4. The dimension of the glass is taken to be 200 mm in span, 20 mm in depth and 10 mm in width. The size of each support is $10 \text{ mm} \times 4 \text{ mm} \times 10 \text{ mm}$. The impactor is just on the top of the glass beam, whose initial velocity is $v_y = -3.13 \text{ m/s}$, size $4 \text{ mm} \times 4 \text{ mm} \times 10 \text{ mm}$ and mass 1.0 kg. For the adaptive model the glass is discretized into 4950 8-node cubic FEs with a size of 2 mm and 100 hexahedral FEs with a size of 1 mm \times 2 mm \times 2 mm; each support 50 cubic FEs with a size of 2 mm; the impactor 20 cubic FEs with a size of 2 mm which are the rigid body elements. For the DE model, the glass is discretized into 40000 spherical DEs with a radius of 0.5 mm.

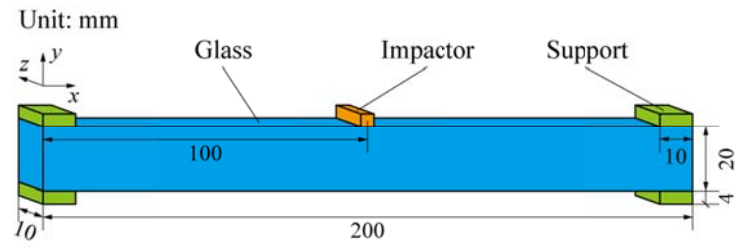


Figure 4. Impact fracture model of the three-point bending beam

The material properties of the three-point bending glass beam model are listed in Table 1. In the numerical simulations the conversion stress is assumed to be 56.0 MPa to guarantee the connective joint type in the DE subregion at the moment when the DEs are generated.

Material Glass Support **Impactor** Density ρ (kg/m³) 2500.0 2400.0 Young's modulus E (GPa) 74.09 5.0 210.0 Poisson's ratio v 0.20.4 0.269Tensile strength σ_t (MPa) 60.0 10.0 Energy release rate G_f (N/m)

0.10

Shear stress factor β

Table 1. Material properties used in the simulation

Based on the theory mentioned above, a numerical code is developed in Fortran 90/95 programming language. The impact fracture procedure of the glass beam is simulated by using the numerical code on a Dell Precision T5810 Workstation. The time step Δ_t is 6×10^{-5} ms small enough to ensure calculation stability for both of the DE and the adaptive models. The physical time is about 100 μ s. The computational time of the 3D adaptive algorithm is about 67s while that of the DEM about 660s. The computational efficiency of the 3D adaptive algorithm is much higher than that of the DEM. Furthermore, almost the same crack patterns are captured as illustrated in Figures 5 and 6.

Figure 5 illustrates the fracture procedure of the glass beam with the DE model. In order to illustrate the damage of the glass the DEs' color is set to be red if the joint model between the DEs is changed from the connective model to the cohesive or the contact models and the main crack is marked by green lines. As shown in Figure 5(a), the glass beam begins to damage at the bottom at about $25\mu s$. Subsequently, one main crack progresses upwards in a very short period of time (about $45\mu s$) to the upper of the glass beam as shown in Figures 5(b) and 5(c) and the crack reaches the opposite

side at about $70\mu s$. Figure 5(d) is the oblique view of the final crack pattern at about $100\mu s$, in which the main crack is surrounded by microcracks and the cohesive zone located in the red region.

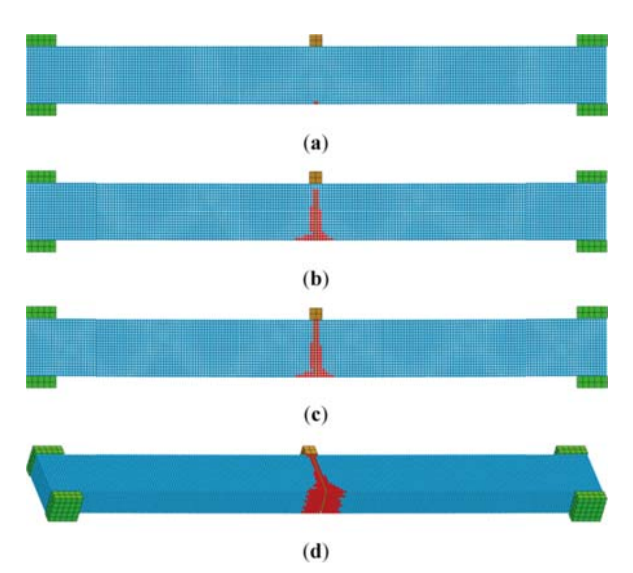


Figure 5. Fracture procedure with the DE model. **a-c** The crack patterns of the middle section by the xy plane: **a** $t = 25\mu s$, **b** $t = 50\mu s$, **c** $t = 70\mu s$; **d** The oblique view of the final crack pattern at about $100\mu s$

Figure 6 illustrates the fracture procedure of the glass beam with the adaptive model. Five finite elements are converted into forty spherical DEs. Following the conversion procedure, the glass beam begins to fracture at the bottom at about $26\mu s$ as shown in Figure 6(a). Subsequently, the conversion procedure progresses upwards in a very short period of time (about $44\mu s$) to the upper of the glass beam and one main crack propagates only in the DE subdomain as shown in Figures 6(b) and 6(c) and the crack reaches the opposite side at about $70\mu s$. Figure 6(d) is the oblique view of the final crack pattern at about $100\mu s$, in which only the main crack is captured in the adaptive model.

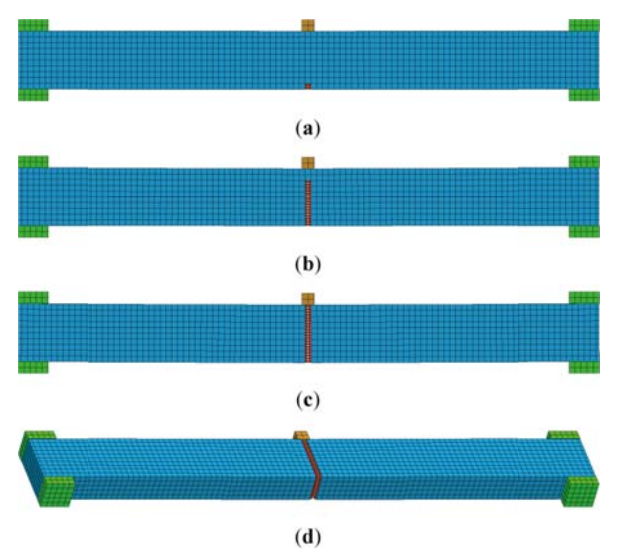


Figure 6. Fracture procedure with the adaptive model. **a-c** The crack patterns of the middle section by the xy plane: $\mathbf{a} \ \mathbf{t} = 26 \mu \mathbf{s}$, $\mathbf{b} \ \mathbf{t} = 50 \mu \mathbf{s}$, $\mathbf{c} \ \mathbf{t} = 70 \mu \mathbf{s}$; \mathbf{d} The oblique view of the final crack pattern at about 100 $\mu \mathbf{s}$

From the above investigations, we notice that the crack paths and the moment of crack occurrence of the adaptive model in Figure 6 are almost unanimous as those of

the DE model in Figure 5. The differences are small; however, one more important characteristic of the 3D adaptive algorithm is the higher computational efficiency.

Conclusion

- (1) A 3D adaptive combined DE/FE algorithm is proposed to analyze the impact fracture problem with a higher computational efficiency.
- (2) The impact fracture of a glass beam is simulated with a higher efficiency by the 3D adaptive algorithm than the DEM. Furthermore, almost the same crack patterns are captured with both numerical methods.

In this work, the same time step is adopted in the FE and the DE subregions and only the cubic FEs can be converted into the spherical DEs. In the future we will overcome these obstacles for more efficiently analyzing the impact fracture of laminated glass with an irregular geometry.

Reference

- Cundall P.A. (1971) A computer model for simulating progressive large scale movements in blocky rock systems. In *Proceedings of the Symposium of the International Society of Rock Mechanics* 1:129-136.
- Foraboschi P. (2007) Behavior and failure strength of laminated glass beams. *Journal of Engineering Mechanics* **133** (12):1290-1301.
- Foraboschi P. (2013) Hybrid laminated-glass plate: Design and assessment. *Composite Structures* **106**:250-263.
- Hidallana-Gamage H., Thambiratnam D., Perera N. (2014) Influence of structural sealant joints on the blast performance of laminated glass panels. *Journal of Performance of Constructed Facilities*, Doi:10.1061/(ASCE) CF.1943- 5509.0000646, 04014151.
- Griffiths D.V., Mustoe G.G.W. (2001) Modelling of elastic continua using a grillage of structural elements based on discrete element concepts. *International Journal for Numerical Methods in Engineering* **50**(7):1759-1775.
- Lei Z., Zang M.Y. (2010) An approach to combining 3D discrete and finite element methods based on penalty function method. *Computational Mechanics* **46**(4):609-619.
- Oda J., Yasuda H. (2007) On impact penetration analysis and evaluation of brittle material plate using three-dimensional DEM (in Japanese). *Journal of Solid Mechanics and Materials Engineering* **1**(3):376-386.
- Shan L., Cheng M., Liu K.X. et al. (2009) New discrete element models for three-dimensional impact problems. *Chinese Physics Letters* **26**(12):120202.
- Zang M.Y., Lei Z., Wang S.F. (2007) Investigation of impact fracture behavior of automobile laminated glass by 3D discrete element method. *Computational Mechanics* **41**(1):73-83.
- Zhang X.H., Hao H., Wang Z.Q. (2015) Experimental study of laminated glass window responses under impulsive and blast loading. *International Journal of Impact Engineering* **78**:1-19.